PERGAMON

International Journal of Solids and Structures 39 (2002) 419–434

INTERNATIONAL JOURNAL OF SOLIDS and STRUCTURES

www.elsevier.com/locate/ijsolstr

A microstructure-based description for cyclic plasticity of pearlitic steel with experimental verification

X. Peng *, J. Fan, Y. Yang

Department of Engineering Mechanics, School of Resources and Environment Science, Chongqing University (A), Chongqing 400044, China

Received 18 October 2000

Abstract

Making use of the microstructure-based constitutive equation for a single dual-phase pearlitic colony and the KBW's self-consistent scheme, a description of dual-phase pearlitic steel is performed. It is based on the assumption that a representative element of the material is an aggregate of numerous spherical pearlitic colonies with randomly distributed orientations, and each colony is composed of many parallel fine lamellas of ferrite and cementite. The corresponding numerical algorithm is developed. The cyclic plasticity of single-phase hard-drawn copper and dual-phase pearlitic steel BS11 subjected to asymmetrically cyclic loading is analyzed and compared with the experimental results. The nonproportional cyclic plasticity of the two materials is also analyzed, in which stress develops along a semi-circle in biaxial tension/compression and shear stress plane, as is experienced by the surface elements in a rolling and sliding contact. The local responses of ferrite and cementite for prescribed orientations are investigated simultaneously. The developed approach can describe the main characteristics in the cyclic plasticity of the dual-phase materials. The corresponding numerical algorithm shows successful stability concerning convergence and accuracy at a large number of cycles.

Keywords: Pearlitic steel; Dual-phase material; Microstructure-based analysis; Constitutive equation; KBW self-consistent scheme; Cyclic plasticity

1. Introduction

Dual-phase pearlitic steel is often used as in rail steel due to its locking-in interphase residual stress capability (Bower, 1989; Bower and Johnson, 1989). When the material is subjected to asymmetric stress cycling, it ratchets in the direction of mean stress, but the ratcheting rate gradually decreases and tends to a steady ratcheting state. Further, if the mean stress is then removed, the material will ratchet in the opposite direction, despite the fact that the mean stress is zero during the following cyclic process (Bower, 1989; Bower and Johnson, 1989, 1990; Peng and Ponter, 1994a). This phenomenon does not appear in

* Corresponding author. Fax: +86-23-6510-6656.
E-mail address: xhpeng@cqu.edu.cn (X. Peng).

0020-7683/01/$ - see front matter
PII: S0020-7683(01)00223-2

single-phase hard-drawn copper, and can be attributed to the special microstructure of the dual-phase material (Bower, 1989; Bower and Johnson, 1989).

Most previous analyses for the mechanical behavior of the dual-phase materials have employed idealized or simplified phenomenological constitutive models, such as those of perfect plasticity or linearly kinematic hardening. The former may overestimate the plastic deformation while the latter may exclude the possibility of a steady accumulation of plastic strain (Bower, 1989). Bower (1989), Bower and Johnson (1990) proposed a constitutive model introducing the second kinematic variable into the Armstrong and Friderick's nonlinear kinematic hardening law (Armstrong and Frederick, 1966), which greatly improved the description for this kind of materials. However, this model cannot predict the steady ratcheting which was observed in experiment (Peng and Ponter, 1994a). It is known that pearlitic steel is composed of a soft phase and a hard phase, and its macroscopic behavior is the combination both phases. A phenomenological dual-phase constitutive model was proposed, with which the behavior of the pearlitic rail steel BS11 under asymmetrical proportional and nonproportional cyclic loading was described (Peng and Ponter, 1994b).

The above mentioned phenomenological constitutive models cannot provide the microstructure dependence of the mechanical behavior of such dual-phase materials (Fan, 1999). It is known that, without in-depth knowledge of the characteristics of the stress and strain evolution in microstructures, issues which exist for a long time in cyclic behavior and fatigue may be difficult to be clarified and solved (McDowell, 1997; Fan, 1999).

A micro/macroscopic analysis for the cyclic plasticity of the dual-phase materials was recently proposed by Fan (1999), where a methodology was developed to simulate the responses of the dual-phase materials based on an important extension of the Hill's self-consistent scheme. This extension considers that a two-phase inclusion is a homogeneous medium in which the detailed microstructure is smeared out. On the other hand, the constitutive relations of the inclusion were obtained from the analysis of interactions of its constituents. The heterogeneity and anisotropy associated with microstructure can, therefore, be accounted for. This is significant because it makes the self-consistent scheme capable of determining the overall responses of materials as well as local stress evolution in microstructures. It showed satisfactory agreement between the predicted and experimental cyclic responses up to 50 cycles. This effort is consistent with the recent understanding that local anisotropy and heterogeneity associated with microstructure have a significant influence on material behavior and fatigue life (McDowell, 1997).

A description for the constitutive behavior of a single pearlitic colony is obtained based on its lamellar microstructure and the assumption that both its ferrite and cementite phases are elastoplastic. Combined with the KBW's self-consistent scheme, the constitutive description of pearlitic steel and the corresponding numerical algorithm are developed. The responses of hard-drawn copper and pearlitic rail steel BS11 subjected to asymmetrical stress cycling are analyzed and compared with experimental results (Bower and Johnson, 1989). Corresponding to the repeated cycles of plastic deformation encountered in rolling and sliding contacts, the responses of copper and BS11 subjected to stress cycles along a semi-circle in biaxial tension/compression and shear stress plane are also analyzed. The proposed approach can also provide the mechanical responses of the material and its two phases in any prescribed orientation.

2. The constitutive model for a pearlitic colony

A pearlitic colony is composed of many fine parallel lamellas of cementite and ferrite (Fig. 1). The thickness of each lamella is assumed to be sufficiently small compared with its in-plane size. So that, the variations of stress and strain in a lamella can be neglected. The in-plane strain components and out-of-plane stress components in all lamellas are, therefore, identical and equal respectively to the corresponding overall strain and stress components of the colony to meet the condition of compatibility, i.e.,

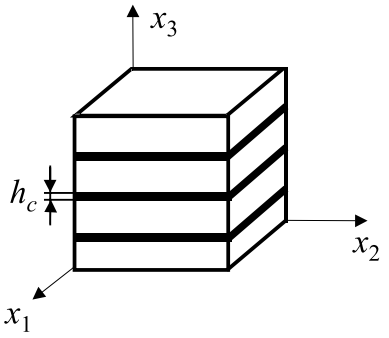

Fig. 1. An element of a pearlitic colony and the local coordinate system.

$$\mathrm{d}\varepsilon_{11}^{\mathrm{c}} = \mathrm{d}\varepsilon_{11}^{\mathrm{f}} = \mathrm{d}\varepsilon_{11} \quad \mathrm{d}\varepsilon_{22}^{\mathrm{c}} = \mathrm{d}\varepsilon_{22}^{\mathrm{f}} = \mathrm{d}\varepsilon_{22} \quad \mathrm{d}\gamma_{12}^{\mathrm{c}} = \mathrm{d}\gamma_{12}^{\mathrm{f}} = \mathrm{d}\gamma_{12}, \tag{1}$$

$$\mathrm{d}\sigma_{33}^{\mathrm{c}} = \mathrm{d}\sigma_{33}^{\mathrm{f}} = \mathrm{d}\sigma_{33} \quad \mathrm{d}\tau_{13}^{\mathrm{c}} = \mathrm{d}\tau_{13}^{\mathrm{f}} = \mathrm{d}\tau_{13} \quad \mathrm{d}\tau_{23}^{\mathrm{c}} = \mathrm{d}\tau_{23}^{\mathrm{f}} = \mathrm{d}\tau_{23}. \tag{2}$$

Assuming both cementite and ferrite being initially isotropic and plastically incompressible, under the condition of isothermal and small deformation, the constitutive equations for a single pearlitic colony and its two phases can be expressed in the following unified form:

$$\{\Delta\sigma^*\} = [D^*]\{\Delta\varepsilon^*\}, \tag{3}$$

where

$$\{\Delta\sigma^*\} = \begin{Bmatrix} \Delta\bar{\sigma}^* \\ \Delta\hat{\sigma}^* \end{Bmatrix}, \quad \{\Delta\varepsilon^*\} = \begin{Bmatrix} \Delta\hat{\varepsilon}^* \\ \Delta\bar{\varepsilon}^* \end{Bmatrix} \quad \text{and} \quad [D^*] = \begin{bmatrix} D_1^* & D_2^* \\ D_3^* & D_4^* \end{bmatrix}, \tag{4}$$

denote incremental stress and strain, and tangential elastoplastic matrix, respectively. For the coordinate system fixed on a pearlitic colony, as shown in Fig. 1, one has the following expressions:

$$\begin{aligned} &\{\Delta\bar{\sigma}^*\} = \left(\Delta\sigma_{11}^*, \Delta\sigma_{22}^*, \Delta\tau_{12}^*\right)^{\mathrm{T}}, \quad \{\Delta\hat{\sigma}^*\} = \left(\Delta\sigma_{33}^*, \Delta\tau_{23}^*, \Delta\tau_{31}^*\right)^{\mathrm{T}}, \\ &\{\Delta\hat{\varepsilon}^*\} = \left(\Delta\varepsilon_{11}^*, \Delta\varepsilon_{22}^*, \Delta\gamma_{12}^*\right)^{\mathrm{T}}, \quad \{\Delta\bar{\varepsilon}^*\} = \left(\Delta\varepsilon_{33}^*, \Delta\gamma_{23}^*, \Delta\gamma_{31}^*\right)^{\mathrm{T}}. \end{aligned} \tag{5}$$

If the superscript "$*$" in the above equations is replaced with "c", "f"and "pc", one obtains the incremental constitutive equations for cementite, ferrite and a single pearlitic colony, respectively.

For a 3-D problem, the elements in $[D^{\mathrm{c}}]$ of cementite (Eq. (4)) can be expressed as

$$\begin{aligned} \left[D_1^{\mathrm{c}}\right] &= \begin{bmatrix} D_{1111}^{\mathrm{c}} & D_{1122}^{\mathrm{c}} & D_{1112}^{\mathrm{c}} \\ D_{2211}^{\mathrm{c}} & D_{2222}^{\mathrm{c}} & D_{2212}^{\mathrm{c}} \\ D_{1211}^{\mathrm{c}} & D_{1222}^{\mathrm{c}} & D_{1212}^{\mathrm{c}} \end{bmatrix}, \quad \left[D_2^{\mathrm{c}}\right] = \begin{bmatrix} D_{1133}^{\mathrm{c}} & D_{1123}^{\mathrm{c}} & D_{1131}^{\mathrm{c}} \\ D_{2233}^{\mathrm{c}} & D_{2223}^{\mathrm{c}} & D_{2231}^{\mathrm{c}} \\ D_{1233}^{\mathrm{c}} & D_{1223}^{\mathrm{c}} & D_{1231}^{\mathrm{c}} \end{bmatrix}, \\ \left[D_3^{\mathrm{c}}\right] &= \begin{bmatrix} D_{3311}^{\mathrm{c}} & D_{3322}^{\mathrm{c}} & D_{3312}^{\mathrm{c}} \\ D_{2311}^{\mathrm{c}} & D_{2322}^{\mathrm{c}} & D_{2312}^{\mathrm{c}} \\ D_{3111}^{\mathrm{c}} & D_{3122}^{\mathrm{c}} & D_{3112}^{\mathrm{c}} \end{bmatrix}, \quad \left[D_4^{\mathrm{c}}\right] = \begin{bmatrix} D_{3333}^{\mathrm{c}} & D_{3323}^{\mathrm{c}} & D_{3331}^{\mathrm{c}} \\ D_{2333}^{\mathrm{c}} & D_{2323}^{\mathrm{c}} & D_{2331}^{\mathrm{c}} \\ D_{3133}^{\mathrm{c}} & D_{3123}^{\mathrm{c}} & D_{3131}^{\mathrm{c}} \end{bmatrix}. \end{aligned} \tag{6}$$

Applying the constitutive model by Fan and Peng (1991), and Peng and Fan (1993) to cementite, each element in Eq. (6) is determined by

$$D_{ijkl}^{\mathrm{c}} = 2\mu^{\mathrm{c}}\delta_{il}\delta_{kj} + \left(K^{\mathrm{c}} - \frac{2}{3}\mu^{\mathrm{c}}\right)\delta_{ij}\delta_{kl} + \frac{T^{\mathrm{c}}}{2G^{\mathrm{c}}\left(f^{\mathrm{c}}(z^{\mathrm{c}})\right)^2}\frac{2(G^{\mathrm{c}} - \mu^{\mathrm{c}})}{H^{\mathrm{c}}}B_{ij}^{\mathrm{c}}\frac{\Delta\eta_{kl}^{\mathrm{c}}}{\Delta z^{\mathrm{c}}}, \tag{7}$$

where η_{ij}^{c} is plastic strain in cementite and $f^{c}(z^{c})$ the hardening function, G^{c} and K^{c} are elastic shear and volumetric moduli of cementite, respectively, and

$$T^{c}=\left(1+\frac{A^{c}}{2G^{c}}\right)^{-1},\quad 2\mu^{c}=A^{c}T^{c}, \tag{8}$$

$$A^{c}=\sum_{r=1}^{n}k_{r}^{c}C_{r}^{c},\quad B_{ij}^{c}(z_{n}^{c})=-\sum_{r=1}^{n}k_{r}^{c}\alpha_{r}^{c}s_{ij}^{c(r)}(z_{n}^{c}), \tag{9}$$

$$H^{c}=1+C^{c}B_{ij}^{c}(z_{n})\eta_{ij}^{c},\quad k_{r}^{c}=\frac{1-\mathrm{e}^{-\alpha_{r}^{c}\Delta z^{c}}}{\alpha_{r}^{c}\Delta z^{c}},\quad C^{c}=\frac{T^{c}}{2G^{c}[f^{c}(z^{c})]^{2}\Delta z^{c}}, \tag{10}$$

$$\Delta s_{ij}^{c(r)}(z^{c})=k_{r}^{c}[C_{r}^{c}\Delta\eta_{ij}^{c}-\alpha_{r}^{c}s_{ij}^{c(r)}(z_{n}^{c})\Delta z^{c}], \tag{11}$$

z^{c} is generalized time which is non-negative and increases monotonically during any plastic deformation due to the following definition of Δz^{c}

$$\Delta z^{c}=\frac{\Delta\zeta^{c}}{f^{c}(z^{c})},\quad (\Delta\zeta^{c})^{2}=\Delta\eta_{ij}^{c}\Delta\eta_{ij}^{c}, \tag{12}$$

z_{n}^{c} is the value of z^{c} after the nth increment of loading and $z^{c}=z_{n}^{c}+\Delta z^{c}$.

The tangential elastoplastic matrix for ferrite can be obtained by replacing the superscript "c" in Eq. (6) through Eq. (12) with "f". The incremental stress and strain satisfy the following relationships

$$\begin{aligned}&\{\Delta\bar{\sigma}^{pc}\}=V\{\Delta\bar{\sigma}^{c}\}+(1-V)\{\Delta\bar{\sigma}^{f}\},\quad \{\Delta\hat{\sigma}^{c}\}=\{\Delta\hat{\sigma}^{f}\}=\{\Delta\hat{\sigma}^{pc}\},\\&\{\Delta\bar{\varepsilon}^{pc}\}=V\{\Delta\bar{\varepsilon}^{c}\}+(1-V)\{\Delta\bar{\varepsilon}^{f}\},\quad \{\Delta\hat{\varepsilon}^{c}\}=\{\Delta\hat{\varepsilon}^{f}\}=\{\Delta\hat{\varepsilon}^{pc}\},\end{aligned} \tag{13}$$

where V denotes the volumetric fraction of cementite. The tangential elastoplastic matrix of a single pearlitic colony can be determined by

$$\begin{bmatrix}D_{1}^{pc} & D_{2}^{pc}\\ D_{3}^{pc} & D_{4}^{pc}\end{bmatrix}=\begin{bmatrix}B_{2}-B_{1}B_{3}^{-1}B_{4} & B_{1}B_{3}^{-1}\\ -B_{3}^{-1}B_{4} & B_{3}^{-1}\end{bmatrix} \tag{14}$$

with

$$\begin{aligned}B_{1}&=VD_{2}^{c}(D_{4}^{c})^{-1}+(1-V)D_{2}^{c}(D_{4}^{c})^{-1},\\B_{2}&=V[D_{1}^{c}-D_{2}^{c}(D_{4}^{c})^{-1}D_{3}^{c}]+(1-V)[D_{1}^{f}-D_{2}^{f}(D_{4}^{f})^{-1}D_{3}^{f}],\\B_{3}&=V(D_{4}^{c})^{-1}+(1-V)(D_{4}^{f})^{-1},\\B_{4}&=-V(D_{4}^{c})^{-1}D_{3}^{c}-(1-V)(D_{4}^{f})^{-1}D_{3}^{f}.\end{aligned} \tag{15}$$

Having derived the incremental stress and strain of a pearlitic colony, the unknown components of the incremental stress and strain of cementite can be calculated by

$$\begin{Bmatrix}\Delta\bar{\sigma}^{c}\\ \Delta\bar{\varepsilon}^{c}\end{Bmatrix}=\begin{bmatrix}D_{2}^{c}(D_{4}^{c})^{-1} & D_{1}^{c}-D_{2}^{c}(D_{4}^{c})^{-1}D_{3}^{c}\\ (D_{4}^{c})^{-1} & -(D_{4}^{c})^{-1}D_{3}^{c}\end{bmatrix}\begin{Bmatrix}\Delta\hat{\sigma}\\ \Delta\hat{\varepsilon}\end{Bmatrix}, \tag{16}$$

and so can those of ferrite.

Note that in Eq. (1), the incremental stress and strain are related to an tangential elastoplastic matrix. This simple relationship will not only bring convenience to the numerical algorithm, but also improve the numerical stability and accuracy under complex loading conditions.

3. KBW's self-consistent scheme

3.1. KBW's self-consistent scheme

Being composed of numerous randomly orientated pearlitic colonies, the constitutive behavior of pearlitic steel can be determined with the constitutive description for a single pearlitic colony as well as by the KBW's self-consistent averaging scheme.

It is known that Hill's self-consistent scheme involves fewer assumptions and may provide a more realistic description. However, it should be mentioned that the corresponding approach is highly implicit and complicated. This is the reason why its first simplification appeared as late as 1979 (Berveoller and Zaoui, 1979). It lost, however, the accuracy of the Hill's weakening constraint capability and can hardly be used for cyclic loading. Fan (1999) made an extension of the scheme, which kept the advantage of the Hill's weakening constraint capability and can be used in more complicated cases. Fan also extended the Hill's scheme to the analysis associated with heterogeneity and anisotropy (Fan, 1999). This contribution is significant and the main concepts will be followed in this paper. On the other hand, computation showed that with the increase of the number of cycles, the numerical stability of the Hill's self-consistent scheme becomes very sensitive to the tolerance error. It can be attributed to the highly implicit property of the Hill's approach. A more reliable algorithm should be developed for the Hill's self-consistent scheme before it is used in the case where a large number of cycles are involved in the computation.

On the contrary, although the KBW's self-consistent scheme employs with a little more assumptions, it yields an explicit and more stable numerical algorithm, which has been validated in the analysis of many problems. The KBW's scheme is adopted in the following analysis. This is due to the fact that our attention is mainly paid to the validity of the proposed constitutive description for the ratcheting behavior of dual-phase pearlitic rail steel in the case of a large number of stress cycles. On the other hand, the constraints of the KBW's scheme can be satisfied in the problem to be discussed.

Consider a representative element of pearlitic steel. It contains a sufficiently large number of randomly orientated pearlitic colonies and in each one the number of lamellas is sufficiently large. The detailed microstructure of the colony is, therefore, smeared out, so that the colony can be regarded as a homogeneous media. With this assumption, one can reasonably obtain the macroscopic stress and strain by volume average over all orientations with a self-consistent scheme (Fan, 1999).

The proposed constitutive description for a single pearlitic colony meets the above assumption. It was built on the basis that the interlamellar spacing is sufficiently small so that the number of the lamellas in a pearlitic colony is sufficiently large. The overall constitutive equation takes a pearlitic colony as a homogeneous media and can describe the mechanical behavior of any part of the colony. On the other hand, it keeps the characteristics of the dual-phase lamellar microstructure and the capability to describe the constitutive behavior of each phase. The combination of the microstructure-based constitutive relationship and the self-consistent scheme yields an across scale of micro/macro description for the constitutive behavior of the dual-phase pearlitic material (Fan, 1999).

The elastic behavior of both phases are assumed isotropic and identical (Langford, 1977). The elastic behavior of the pearlitic colony is, therefore, uniform and isotropic. This is important for the application of the KBW's averaging scheme (Budiansky and Wu, 1962; Kroner, 1961). In the following, each pearlitic colony is assumed as an effective homogeneous sphere and is embedded in a homogeneous medium with the macroscopic property of the dual-phase pearlitic steel.

Assuming that a pearlitic colony and the representative element of pearlitic steel are plastically incompressible, in the case of isothermal and small deformation, the KBW's self-consistent scheme gives (Budiansky and Wu, 1962; Kroner, 1961)

$$\Delta\sigma^{pc} - \Delta\sigma = -\alpha(\Delta\eta^{pc} - \Delta\eta), \tag{17}$$

where $\Delta\sigma^{pc}$ and $\Delta\eta^{pc}$ are respectively the increments of stress and plastic strain of a single pearlitic colony, $\Delta\sigma$ and $\Delta\eta$ the average overall incremental stress and plastic strain, G elastic shear modulus of the material, and α is determined by

$$\alpha = \frac{2(7-5v)}{15(1-v)}G, \tag{18}$$

where v is the Poisson's ratio. It is easily obtained from Eq. (17) that

$$\Delta\sigma_{kk}^{pc} = \Delta\sigma_{kk}, \quad \Delta s^{pc} - \Delta s = \Delta\sigma^{pc} - \Delta\sigma, \tag{19}$$

where Δs^{pc} and Δs are the incremental deviatoric stresses in a single colony and the aggregate, respectively. Making use of

$$\Delta\eta^{pc} = \Delta\varepsilon^{pc} - \frac{1}{3}\mathrm{tr}(\Delta\varepsilon^{pc})I_2 - \frac{\Delta s^{pc}}{2G}, \quad \Delta\eta = \Delta\varepsilon - \frac{1}{3}\mathrm{tr}(\Delta\varepsilon)I_2 - \frac{\Delta s}{2G} \tag{20}$$

and Eq. (19), one derives the following equation

$$\gamma(\Delta\sigma^{pc} - \Delta\sigma) = -\alpha(\Delta\varepsilon^{pc} - \Delta\varepsilon) \tag{21}$$

with

$$\gamma = 1 - \frac{\alpha}{2G} = \frac{2(4-5v)}{15(1-v)}. \tag{22}$$

From Eq. (21), one can easily define the following invariant

$$\Delta q = \gamma\Delta\sigma + \alpha\Delta\varepsilon = \gamma\Delta\sigma^{pc} + \alpha\Delta\varepsilon^{pc}. \tag{23}$$

Substituting the constitutive equation for a single pearlitic colony Eq. (3) into Eq. (23) yields

$$\{\Delta q\} = [\gamma[D^{pc}] + \alpha[I]]\{\Delta\varepsilon^{pc}\}. \tag{24}$$

In the above equations, the macroscopic plastic strain increment $\Delta\eta$ is related to the plastic strain increment of each colony $\Delta\eta^{pc}$ by a certain averaging procedure, i.e.,

$$\Delta\eta = \langle\Delta\eta^{pc}\rangle \tag{25}$$

and the following relationships can easily be derived from Eqs. (17) and (21)

$$\Delta\sigma = \langle\Delta\sigma^{pc}\rangle \quad \text{and} \quad \Delta\varepsilon = \langle\Delta\varepsilon^{pc}\rangle. \tag{26}$$

3.2. Averaging procedure

A mixed averaging procedure was used for polycrystalline analysis by Zeng (1996), Peng et al. (1997), and Peng and Fan (2000). It is based on an isosahedron: the outer normal directions of the 20 faces determine 20 spatially uniformly distributed orientations represented by 20 sets of θ_i and ϕ_i $(i = 1, 2, \ldots, 20)$, and in each face it is assumed that there are numerous single pearlitic colonies with randomly distributed orientations, i.e., ω varies continuously (see Fig. 2). If the arithmetic averaging procedure is used for θ_i and ϕ_i $(i = 1, 2, \ldots, 20)$ and integral averaging for ω, making use of the Gaussian quadrature and noticing the symmetry of the problem, the averaging procedure Eq. (26) can be specified as (Peng and Fan, 2000)

$$\Delta\varepsilon = \frac{1}{20}\sum_{i=1}^{10}\sum_{j=1}^{4}A_j^{\omega}\Delta\varepsilon^{pc}(\theta_i, \phi_i, \omega_j), \tag{27}$$

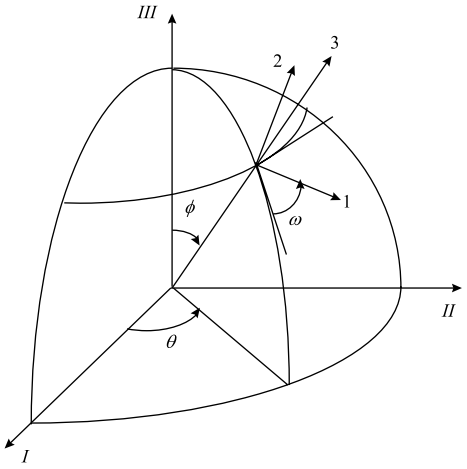

Fig. 2. Global and local coordinate systems.

Table 1
Coordinates of Gaussian integral points ω_j and weighted coefficients A_j^{ω}

j	1	2	3	4
ω_j (rad)	0.1090633	0.5183777	1.052419	1.461733
A_j^{ω}	0.3478548	0.6521452	0.6521452	0.3478548

Table 2
Values of the independent 10 sets of θ_j and ϕ_j

j	1	2	3	4	5	6	7	8	9	10
$\theta_j(^\circ)$	0	72	144	216	288	0	72	144	216	288
$\phi_j(^\circ)$	37.38	37.38	37.38	37.38	37.38	79.19	79.19	79.19	79.19	79.19

where the coordinates of the Gaussian integration points ω_j and the corresponding weighted coefficients A_j^{ω} are listed in Table 1, and the values of the 10 sets of independent θ_i and ϕ_i $(i = 1, 2, \ldots, 10)$ are listed in Table 2.

The above averaging procedure, in general, involves the response of 40 single pearlitic colonies with different orientations even if the improvement by the Gaussian weighed coefficients is not considered. Analysis shows that this mixed procedure provides a satisfactory accuracy in the analysis of polycrystalline response because of its spatially uniform distribution of the orientations determined by the chosen θ_i and ϕ_i (Peng and Fan, 2000). In the analysis for the aggregate of pearlitic colonies, the numerical process becomes simpler, because the mechanical property is independent of ω if the coordinate system 123 in Fig. 1 is identical with the local coordinate system 123 in Fig. 2. It implies that the overall constitutive behavior of pearlitic steel can be obtained in average by using 10 colonies with the prescribed orientations θ_i and ϕ_i.

4. Application and verification

A numerical procedure for the analysis of the cyclic plasticity of dual-phase pearlitic materials subjected to a given stress history is proposed as follows:

With the result obtained in the kth iteration of the nth increment of loading $\Delta\sigma_{(n)}$, such as $\Delta\varepsilon_{(n)}^{(k)}$ of the material, $\Delta\varepsilon_{(n)}^{\mathrm{pc}(k)}$ and $\Delta\sigma_{(n)}^{\mathrm{pc}(k)}$ of each single pearlitic colony, $\Delta\varepsilon_{(n)}^{\mathrm{c}(k)}$, $\Delta\sigma_{(n)}^{\mathrm{c}(k)}$ of the cementite and $\Delta\varepsilon_{(n)}^{\mathrm{f}(k)}$, $\Delta\sigma_{(n)}^{\mathrm{f}(k)}$ of the ferrite in the colony can be calculated, $[D^{\mathrm{pc}}]$ of each single colony can be modified with Eq. (14). With the given increment of stress, $\Delta q_{(n)}^{(k+1)}$ can be calculated using Eq. (23), for each colony $\Delta\varepsilon_{(n)}^{\mathrm{pc}(k+1)}$ can be solved from Eq. (24), and $\Delta\sigma_{(n)}^{\mathrm{pc}(k+1)}$ can be calculated with Eq. (3). Then, $\Delta\varepsilon_{(n)}^{(k+1)}$ is obtained with Eq. (27), $\Delta\varepsilon_{(n)}^{\mathrm{c}(k+1)}$, $\Delta\sigma_{(n)}^{\mathrm{c}(k+1)}$ and $\Delta\varepsilon_{(n)}^{\mathrm{f}(k+1)}$, $\Delta\sigma_{(n)}^{\mathrm{f}(k+1)}$ with Eq. (16). The iterative process continues until the maximum relative error δ satisfies

$$\delta = \max_{j=1}^{N'} \frac{\|\Delta q_{(n)}^{(k+1)} - \Delta q_{(n)}^{(k)}\|}{\|\Delta q_{(n)}^{(k+1)}\|} \leqslant \delta_0, \tag{28}$$

where N' is the number of colonies used in the computation and δ_0 is the tolerance, $\delta_0 = 0.001$ being prescribed in computation. Then, the obtained incremental results are superimposed respectively on the corresponding results up to the $(n-1)$th increment of loading and one starts, therefore, the computation for the next increment of loading.

4.1. Responses of BS11 and copper subjected to asymmetrical uniaxial cyclic stress

The responses of rail steel BS11 subjected to asymmetrical proportional and nonproportional cyclic stress (Bower, 1989) are analyzed with the proposed approach. The responses of single-phase hard-drawn copper subjected to asymmetrical stress cycling are also analyzed for comparison.

The material constants of the two materials are identified with the experimental results using trial and error method and shown in Table 3. $n = 2$ is used for the ferrite and cementite phases of BS11, respectively, and $n = 3$ for the hard-drawn copper to satisfy the requirement of both accuracy and efficiency in engineering application. The hardening function

$$f^{\mathrm{c}}(z^{\mathrm{c}}) = d^{\mathrm{c}} - (d^{\mathrm{c}} - 1)\mathrm{e}^{-\beta^{\mathrm{c}} z^{\mathrm{c}}} \tag{29}$$

is used for cementite. The hardening function for ferrite can be obtained from Eq. (29) by replacing the superscript "f" with "c". If the material involves considerable additional hardening caused by nonproportional cyclic loading, the corresponding additional hardening factor can be introduced into the hardening function without difficulty, as was proposed by Fan and Peng (1991). However, it will be ignored in the following computation because of insufficient experimental evidence.

For hard-drawn copper, the material constants can be identified using a uniaxial stress–plastic strain curve by following the procedure used by Fan and Peng (1991) with a curve-fitting program.

For a dual-phase material, in principle, the material constants of each phase should be identified independently with the above procedure. It is, however, difficult because it is hard and even impossible to separate the two phases from each other and obtain the mechanical property of each phase independently. In view of engineering application and considering the effect of grain boundary and other defects, the material constants can be identified with the experimental macroscopic stress–strain curve and a curve-

Table 3
Material constants

Materials	G (GPa)	v	C_1, C_2, C_3 (GPa)	α_1, α_2, α_3	d	β
BS11						
Ferrite	80	0.3	186.5, 1.5,	500, 60,	1.0	–
Cementite			24 000, 1500,	30 000, 2000,	3.3	4.5
Copper	47.7	0.3	308, 49.2, 5.2	3000, 800, 90	1.0	–

fitting program. Fortunately, the measured volume fraction of cementite and the estimates of the strengths of ferrite and cementite (Langford, 1977; Park and Bernstein, 1979) provide available constraints to identify the material constants.

Bower's experimental results (Bower, 1989) are simulated. The cylindrical specimen, which was used in experiment, has a diameter and length of the working part of 9.525 mm (3/8 in.) and 19.05 mm (3/4 in.), respectively. The axial displacement was recorded by a displacement transducer mounted between grips (Bower, 1989).

The computed load-extension curve of the hard-drawn copper specimen subjected to asymmetric cyclic stress is shown in Fig. 3(b), where the mean and amplitude of load are $P_m = 500$ N and $P_a = 3750$ N, respectively, with a stress rate of ± 1.25 kN/s. The experimental measurement (Bower, 1989) is given in Fig. 3(a). The comparison between the computed and experimental results shows a satisfactory agreement except for the first few cycles. The error can be mainly attributed to the difference between the responses of monotonic and cyclic loading and the unstable material property in the first few cycles, which cannot be well described with unified material constants. Difference between the slopes of the computed and experimental curves can be detected. It can be attributed to the involvement of elastic deformation of the rest part of the specimen, which is included in the experimental measurement but excluded from the computation. It can be seen in Fig. 3(a) that the ratcheting rate varies in the first few cycles and quickly tends to a constant, which is well replicated in the computation. It should be noted that since the copper is a single-phase isotropic material, the mechanical property of each "colony" is independent of the orientation, and identical with that of the representative material element. Although, the program with the KWB's scheme is used for the analysis, it involves a unique cell (or colony). The averaging scheme, thus, does not work.

Fig. 4 shows the extension of the BS11 specimen subjected to the asymmetrical cyclic tensile/compressive load with mean $P_m = 1$ kN, amplitude $P_a = 10$ kN and the stress rate ± 3.33 kN/s. Compared with the

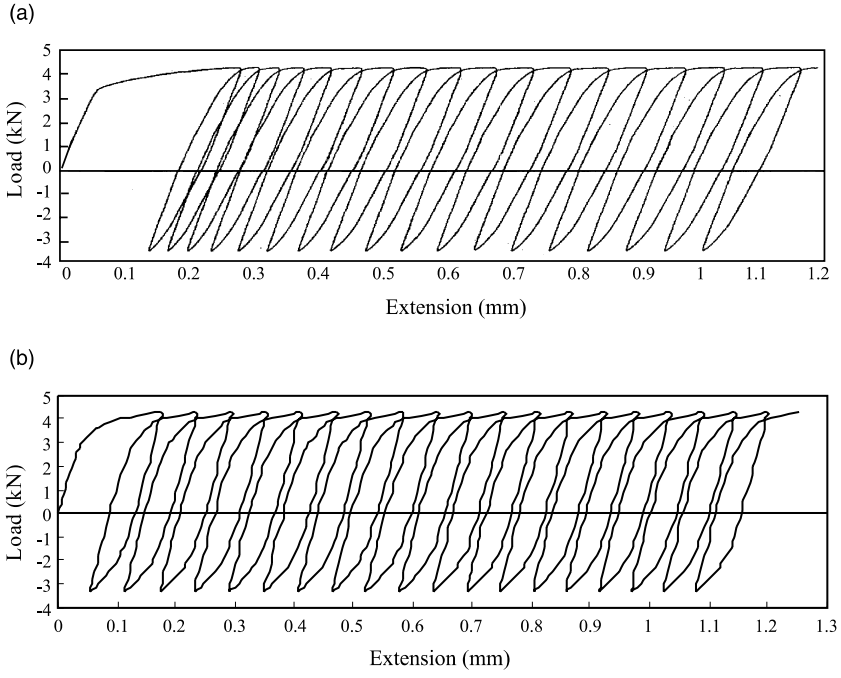

Fig. 3. Response of the hard-drawn copper specimen under tensile cyclic stress. (a) Experimental, (b) computational.

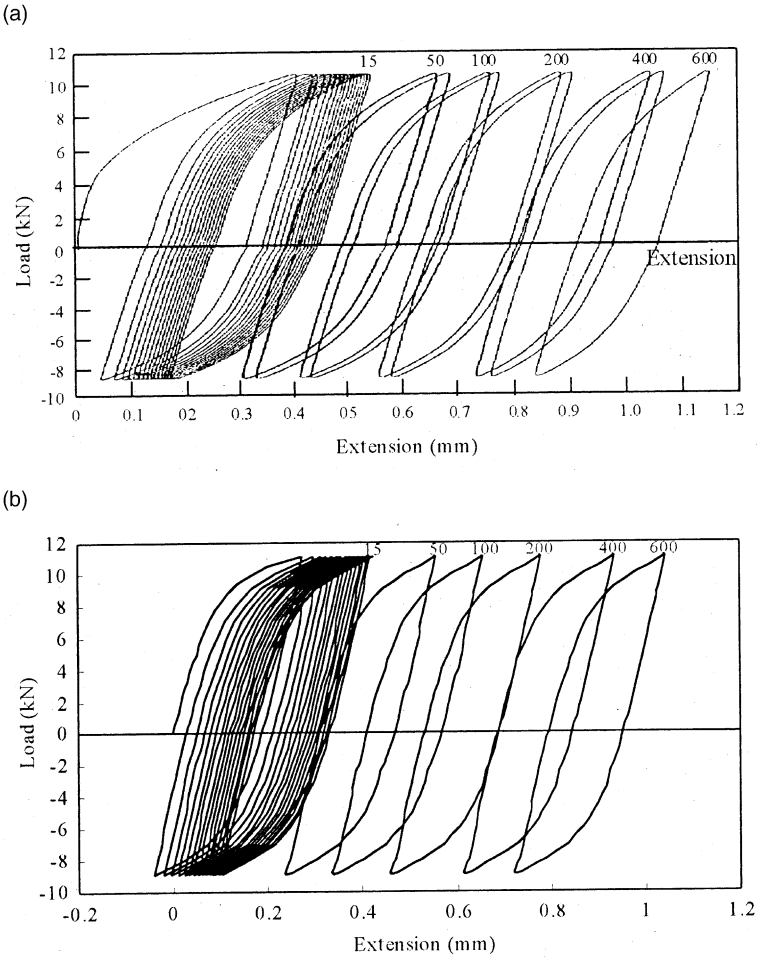

Fig. 4. Responses of BS11 specimen under asymmetrical stress cycling. (a) Experimental, (b) computational.

experimental result, Fig. 4(a) shows that the ratcheting rate and its variation with the increase of the number of cycles. Fig. 5 points out the variation of the ratcheting elongation against the number of cycles (see Fig. 4). It can be found that the proposed approach provides a better description for the experimental result compared with Bower's model (Bower, 1989).

4.2. Responses of BS11 and copper subjected to nonproportional cyclic stress

Surfaces that are in rolling and sliding wheel/rail contact almost inevitably suffer from some degree of plastic deformation. A great deal of experimental evidence has shown that fatigue cracks can be initiated in zones where the plastic deformation is localized near to the free surface. An understanding of the plastic deformation is an important step towards developing theories of wear and of fatigue crack initiation (Bower and Johnson, 1989). Assuming the two contact surfaces are topographically smooth and restricting the discussion to plane-strain problem, the contact pressure between a cylinder and the half-space remains approximately Hertzian, the normal and tangential traction were expressed as (Bower and Johnson, 1989)

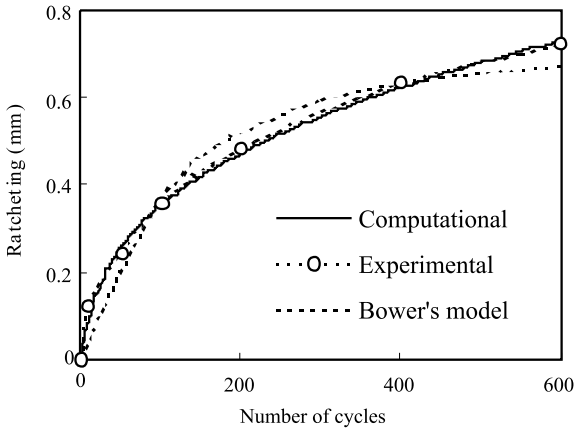

Fig. 5. Accumulated elongation against the number of stress cycles.

$$p = p_0\sqrt{1-(x/a)^2}, \quad q = \mu p, \tag{30}$$

where p_0 is the peak Hertzian pressure, a the contact half-width and μ the friction coefficient. It is known that the elastic stresses at the contact surface due to the Hertzian pressure (Eq. (30)) comprise equal biaxial compression $\sigma_{xx} = \sigma_{zz} = -p$ (Bower and Johnson, 1989). Any tendency of lateral plastic deformation is resisted when $\sigma_{yy} = -p$, i.e., the stress state is hydrostatic and does not give rise to further plastic deformation in any plane. Plastic flow is therefore governed by the frictional traction Eq. (30) that gives rise to the following stress components inside contact area,

$$\sigma_{xx} = -2\mu p_0 x/a, \quad \tau_{xz} = -\mu p_0\sqrt{1-(x/a)^2}, \quad |x| \leqslant a. \tag{31}$$

The corresponding principal shear stress in the plane of deformation is

$$\tau = \sqrt{\left(\frac{1}{2}\sigma_{xx}\right)^2 + \tau_{xz}^2} = \mu p_0. \tag{32}$$

It can be seen that the locus of stress is a semi-circle in the plane $(\frac{1}{2}\sigma_{xx}, \tau_{xy})$ with μp_0 as its radius (see Fig. 6(a)), which is typically asymmetrical and nonproportional.

The responses of BS11 and copper subjected to cyclic stressing along a biaxial semi-circle are shown in Fig. 6(c) and (d), respectively, where $\mu p_0 = 231$ MPa for BS11 and $\mu p_0 = 100$ MPa for copper. With copper, the longitudinal strain ε_{xx} oscillates between about -0.181% and 0.402%, but it ratchets in the γ_{xz} direction with almost constant rate $\mathrm{d}\gamma_{xz}/\mathrm{d}N = 0.26\%$. With BS11 the longitudinal strain ε_{xx} oscillates between unstable limits in the initial stage due to the unstable nature and complicated interaction between phases and colonies but the bounds tend to be stable with limits between about -0.331% and 0.632%. The ratcheting in the direction of γ_{xz} is shown in Fig. 6(b), where the ratcheting rate keeps decreasing with increasing the number of cycles. It may be conjectured that the ratcheting rate could be sufficiently small with a large cyclic number.

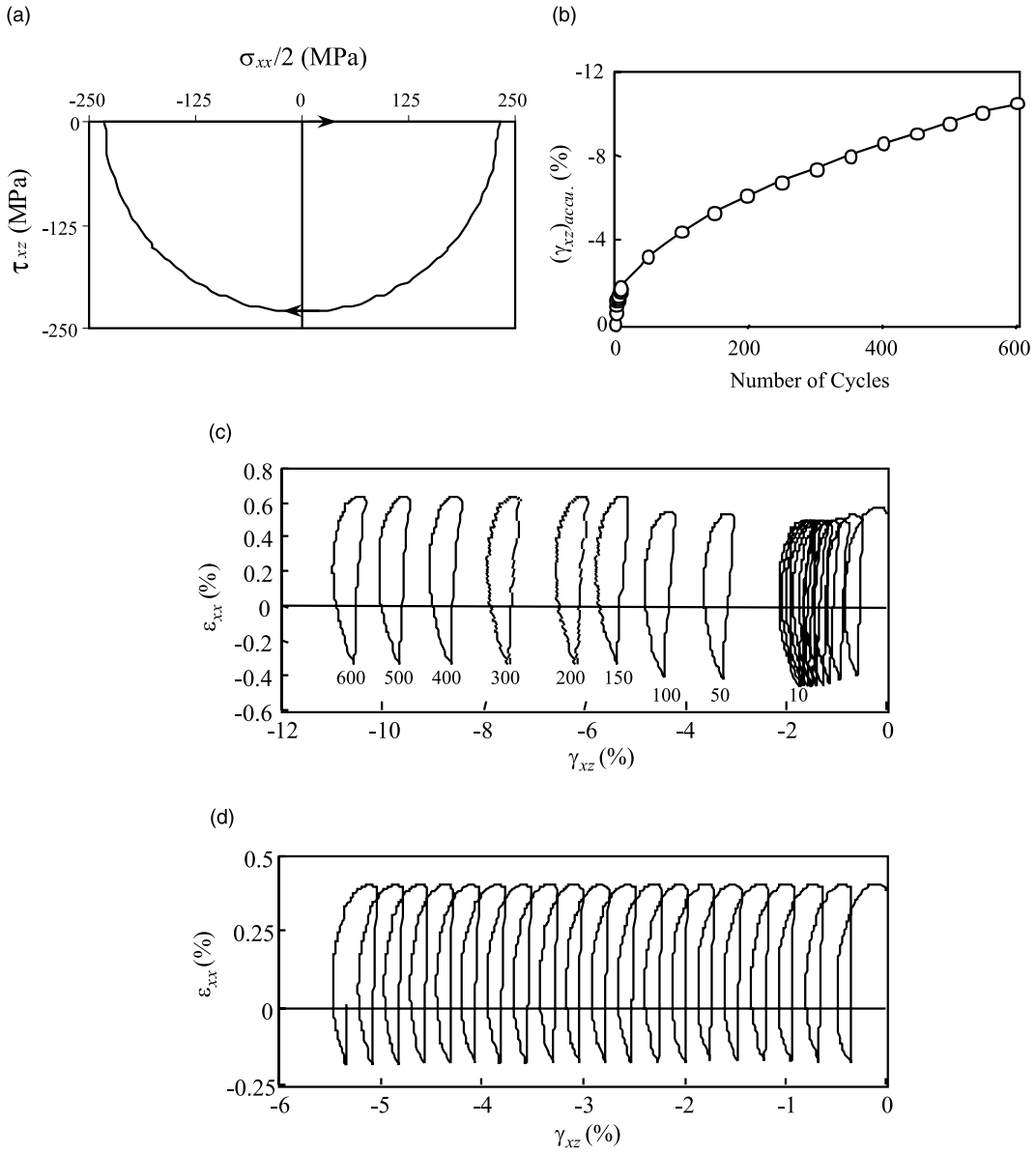

Fig. 6. Simulation of the responses of surface material under rolling and sliding contact. (a) Semi-circle stress lotus, (b) ratcheting of BS11, (c) strain lotus of BS11, (d) strain lotus of copper.

4.3. Local responses of ferrite and cementite with prescribed orientations

The equivalent stress is defined as follows:

$$\sigma_e = \sqrt{\frac{1}{2}[(\sigma_{11}-\sigma_{22})^2 + (\sigma_{22}-\sigma_{33})^2 + (\sigma_{33}-\sigma_{11})^2 + 6(\tau_{12}^2+\tau_{23}^2+\tau_{31}^2)]}. \tag{33}$$

The variations of equivalent and volumetric stresses in the ferrite and cementite in the colonies with the 10 prescribed orientations (Table 2) are investigated and shown in Figs. 7 and 8, respectively. The BS11 specimen is subjected to asymmetrical axial cyclic stress σ_{xx} with mean $(\sigma_{xx})_m = 56.5$ MPa and amplitude $(\sigma_{xx})_a = 561.5$ MPa, and the overall response has been shown in Fig. 4. The four columns in each group in Figs. 8 and 9 correspond to the responses at the upper peak of the macroscopic stress $(\sigma_{xx})_{max} = 618$ MPa in cycles 10, 50, 200, 600, respectively.

Fig. 7(a) shows the equivalent stresses σ_e in the ferrite of the 10 colonies. It can be seen that they are almost identical and do not change obviously during the cyclic process. The values of these equivalent stresses are very close to the limit strength of ferrite, which indicates plastic deformation taking place in the ferrite in each pearlitic colony in the corresponding cyclic stress. In Fig. 7(b), distinct differences can be observed between the equivalent stresses in the cementite in different pearlitic colonies. Distinct change of them can also be observed during this loading.

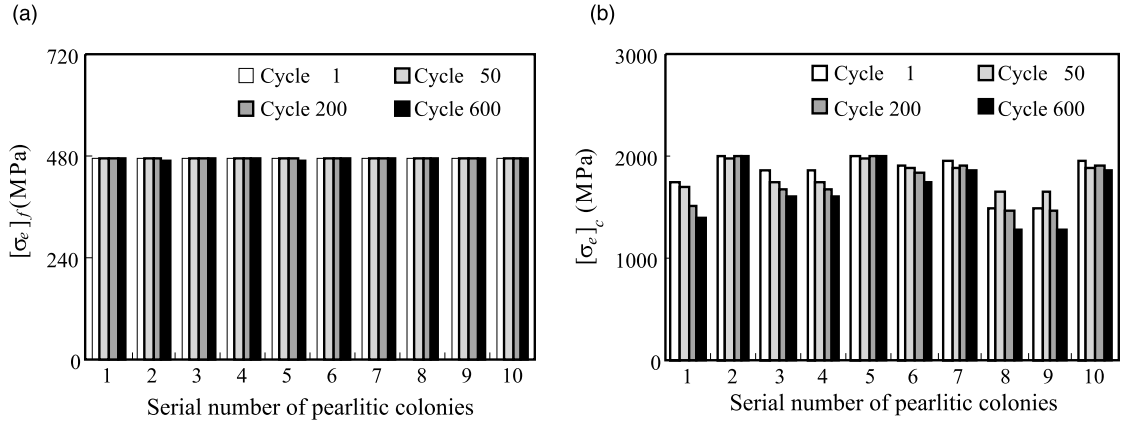

Fig. 7. Distributions of σ_e in the ferrite and cementite of the pearlitic colonies of prescribed orientations (a) σ_e in ferrite, (b) σ_e in cementite.

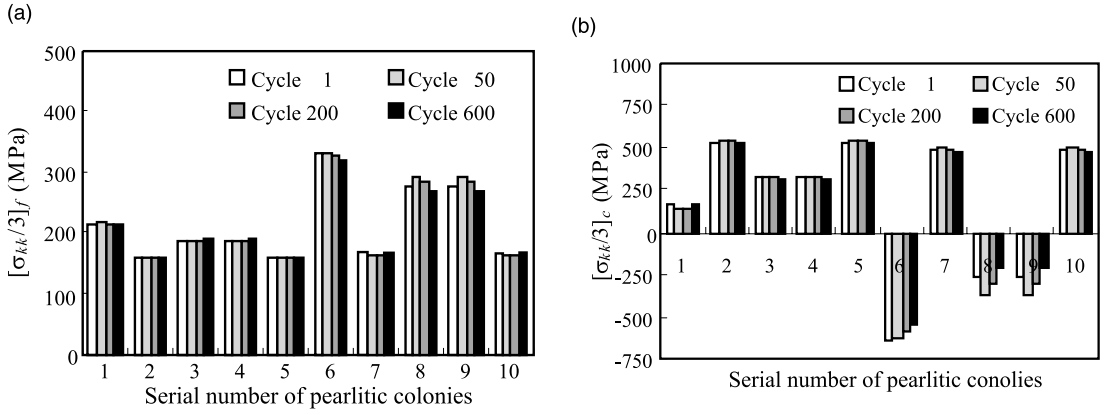

Fig. 8. Distributions of $\sigma_{kk}/3$ in the ferrite and cementite of the pearlitic colonies of prescribed orientations, (a) $\sigma_{kk}/3$ in ferrite, (b) $\sigma_{kk}/3$ in cementite.

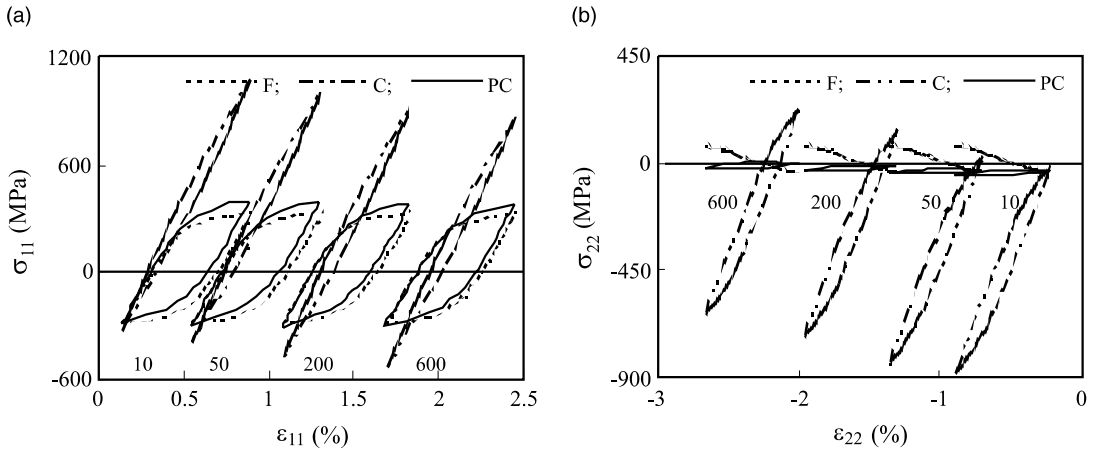

Fig. 9. Hysteresis loops of pearlitic colony 1 during overall asymmetric cyclic loading, (a) σ_{11}–ε_{11} loops, (b) σ_{22}–ε_{22} loops.

Some important differences in the volumetric stresses of ferrite between the colonies with different orientations are well demonstrated in Fig. 8(a), and so for those of cementite (Fig. 8(b)). Larger positive volumetric stresses exist in colonies 6, 8 and 9, while the negative volumetric stresses are found in the cementite of these colonies. Analysis shows that these three colonies undergo larger tensile stress in the direction 3 of their local coordinate systems (Fig. 1). The constraint between the neighboring ferrite and cementite lamellas can account for such distributions of local volumetric stress. It is known that large tensile volumetric stress in ferrite easily results in damage, which should be avoided in practice.

Fig. 9 shows the hysteresis loops of some stress–strain components in the colony with orientation 1 (Table 2), which correspond to cycles 10, 50, 200 and 600 of BS11 subjected to asymmetrical cyclic stress σ_{xx} varying between 56.5 ± 561.5 MPa. Fig. 9(a) shows the in-plane σ_{11}–ε_{11} hysteresis loops, where $\varepsilon_{11}^{f} = \varepsilon_{11}^{c} = \varepsilon_{11}^{pc}$, but the variation of the corresponding stress component in cementite is much larger than that in ferrite. On the other hand, a positive mean value of this stress component is found in cementite, which decays significantly during cyclic loading. Correspondingly, the ratcheting rate in this direction is also greatly reduced. It can be found in Fig. 9(b) that, in the in-plane σ_{22}–ε_{22} hysteresis loops, the stress

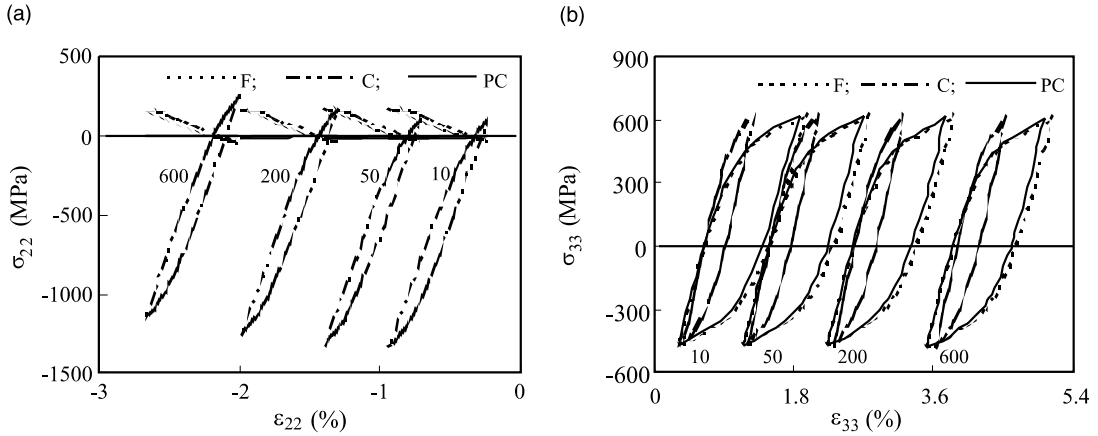

Fig. 10. Hysteresis loops of pearlitic colony 6 during overall asymmetric cyclic loading, (a) σ_{11}–ε_{11} loops, (b) σ_{33}–ε_{33} loops.

components in ferrite and cementite develop in the opposite direction, and the variation in the latter is much faster. With the decrease of the mean of the stress component in cementite, the mean of the corresponding stress component in the pearlitic colony decreases and gradually vanishes.

Fig. 10(a) shows the in-plane σ_{22}–ε_{22} hysteresis loops of the pearlitic colony with orientation 6 (Table 2). It is similar to that shown in Fig. 9(b). The in-plane σ_{11}–ε_{11} hysteresis loops show the similar tendency. The out-of-plane σ_{33}–ε_{33} hysteresis loops are given in Fig. 10(b), where it is seen that $\sigma_{33}^{f} = \sigma_{33}^{c} = \sigma_{33}^{pc}$. Although σ_{33}^{c} does not seem very high, remarkable plastic strain component and ratcheting are detected in cementite in the corresponding direction due to its large equivalent stress (Fig. 7(b)).

5. Conclusions and discussion

A microstructure-based constitutive model was obtained for a single pearlitic colony. With this model and the KBW's self-consistent scheme, a constitutive description for typical dual-phase pearlitic steel was developed. The cyclic plasticity of BS11 and copper subjected to asymmetrical cyclic stress and strain histories were analyzed and compared with experimental results. Both proportional and nonproportional cases are involved.

As a single-phase material, the hard-drawn copper ratchets at an almost uniform rate when it is subjected to asymmetrical stress cycling. On the contrary, as a dual-phase material, BS11 ratchets at a decreasing rate. These characteristics were satisfactorily reproduced.

Corresponding to the repeated cycles of plastic deformation encountered in rolling and sliding contacts, the responses of copper and BS11 subjected to stress cycles along a semi-circle path in biaxial tension/compression and shear stress plane were analyzed. It can be seen that, for the hard-drawn copper, ratcheting develops in the direction of mean shear stress with an almost constant rate. But for BS11, the shear strain accumulates at a decreasing rate. This particular ratcheting behavior of BS11 can be attributed to its locking-in interphase residual stress capability. It is related to the inconsistency of the deformation and the interaction between different phases, which can be accounted for by the proposed microstructure-based description.

The KBW's self-consistent scheme was used to obtain the overall response of pearlitic steel to avoid the complexity and the numerical sensitivity of Hill's self-consistent scheme. This is acceptable because a pearlitic colony can be reasonably assumed as a spherical inclusion and the elastic properties of the material and its colonies can be regarded isotropic and identical with each other. The tangential elastoplastic matrix which relates the overall increments of stress and strain can be conveniently combined with the self-consistent scheme to generate an algorithm with high accuracy and efficiency. With the proposed constitutive relationship the representative cell of a single pearlitic colony can be considered homogeneous ignoring its detailed microstructure and embedded in a homogeneous medium. On the other hand, the response of any single colony and the local responses of ferrite and cementite with any prescribed orientation can also be obtained simultaneously. Since marked difference may exist between the local and overall material properties and between the local and overall states of stress, the microstructure-based analysis might be of particular significance in the development of the corresponding microstructure-based damage and failure analysis.

Acknowledgements

The authors gratefully acknowledge the financial support to this work from the Natural Science Foundation of China and Education Ministry of China.

References

Armstrong, R.J., Frederick, C.O., 1966. A mathematical representation of the multiaxial Bauschinger effect. Report/RD/B/N 731. General Electricity Generating Board.

Berveoller, M., Zaoui, A., 1979. An extension of the self-consistent scheme to plastically flowing polycrystals. J. Mech. Phys. Solids 26, 325–344.

Bower, A.F., 1989. Cyclic hardening properties of hard-drawn copper and rail steel. J. Mech. Phys. Solids 37, 455–470.

Bower, A.F., Johnson, K.L., 1989. The influence strain hardening on cumulative plastic deformation in rolling and sliding contact. J. Mech. Phys. Solids 37, 471–493.

Bower, A.F., Johnson, K.L., 1990. Plastic flow and shakedown of rail surface in repeated wheel-rail contact. In: 3rd Int. Symp. Contact Mech. & Wear of Wheel–Rail Systems, Cambridge, UK.

Budiansky, B., Wu, T.T., 1962. Theoretical prediction of plastic strain of polycrystals. In: Proc 4th US National Congr. Appl. Mech., pp. 1175–1185.

Fan, J., Peng, X., 1991. A physically based constitutive description for nonproportional cyclic plasticity. J. Engng. Mater. Technol. 113, 254–262.

Fan, J., 1999. A micro/macroscopic analysis for cyclic plasticity of dual-phase materials. J. Appl. Mech. 66, 124–136.

Kroner, E., 1961. Zur Plastichen verformung des vielkristalls. Acta Metall. 9, 155–165.

Langford, G., 1977. Deformation of pearlite. Metall. Trans. A 8, 861–875.

McDowell, D.L., 1997. An engineering model for propagation of small crack in fatigue. Engng. Fract. Mech. 56 (3), 357–377.

Park, Y.J., Bernstein, I.M., 1979. The process of crack initiation and effective grain size for cleavage fracture in pearlitic eutectoid steel. Metall. Trans. A 10, 1653–1663.

Peng, X., Fan, J., 1993. A numerical approach for nonclassical plasticity. Comput. Struct. 47, 313–320.

Peng, X., Ponter, A.R.S., 1994a. An experimental investigation of the response of BS11 steel to cyclic loading. Int. J. Solids Struct. 31, 807–833.

Peng, X., Ponter, A.R.S., 1994b. A constitutive law for a class of two-phase materials with experimental verification. Int. J. Solids Struct. 31, 1099–1111.

Peng, X., Zeng, X., Fan, J., 1997. On a nonclassical constitutive theory of crystal plasticity. Mech. Res. Commun. 24, 631–638.

Peng, X., Fan, J., 2000. A new approach to the analysis of polycrystal plasticity. Arch. Mech. 52, 103–125.

Zeng, X., 1996. Microscopic and phenomenological study of polycrystal plasticity and creep. Ph.D. dissertation, Chongqing University.